The Micro-Optical Ring Electrode. 3: Transient Photocurrent Studies of Photophysical−Electrochemical and Photophysical−Chemical−Electrochemical Systems†

Fabrice P. L. Andrieux,‡ Colin Boxall,*,‡ and Danny O'Hare§

Centre for Materials Science, University of Central Lancashire, Preston PR1 2HE, U.K., and Department of Bioengineering, Imperial College, London SW7 2BP, U.K.

Received: April 12, 2006; In Final Form: June 22, 2006

The micro-optical ring electrode (MORE) is a photoelectrochemical device based on a ring microelectrode that uses the insulating material interior to the ring electrode as a light guide. In this paper, we describe the preparation and characterization of very thin ring MOREs with (ring inner radius)/(ring outer radius) > 0.99. Theoretically, we derive asymptotic analytical expressions for the time dependence of the diffusion-limited transient light-on photocurrent generated by two general types of photoelectrochemical systems: (a) the PE (photophysical−electrochemical) system, wherein the photoexcited species itself is directly detected on the ring; (b) the PCE (photophysical−chemical−electrochemical) system, wherein the photoexcited species undergoes a homogeneous electron transfer reaction prior to electrochemical detection. Experimentally, we establish that it is possible to use such MOREs to study the wavelength dependence of photocurrents derived from photoelectrochemically active systems, such as the $Ru(bipy)_3^{2+}/Fe^{3+}$ PCE system, demonstrating the potential utility of the MORE as a selective electroanalytical probe. We also use our expressions for the time dependence of photocurrents at the MORE to derive values for the photoelectrochemical kinetic parameters of this system, including the rate coefficient for the back reaction of photogenerated $Ru(bipy)_3^{3+}$ ($0.115\ s^{-1}$) and the quantum efficiency for the primary redox products, $Ru(bipy)_3^{3+}$ and Fe^{2+}, escaping cage recombination, $\phi_{CE} = 0.099$.

1. Introduction

Photoelectrochemistry is a vigorously advancing research front owing to its range of applications in solar energy conversion,[3−6] organic and inorganic pollution abatement,[7,8] self-cleaning materials,[9] nonlinear optics,[10] and the development of photoactive drugs.[11] Many of the processes underlying these applications involve the photogeneration of electrochemically active, short-lived species whose electrochemistries it would be desirable to interrogate for purposes of system optimization. There is therefore a need for a quantitative device capable of studying photoelectrochemistries on the time scale of microseconds or faster.

One such device is the micro-optical ring electrode (MORE, Figure 1). On the basis of a ring microelectrode and using the insulator interior to the ring as a light guide, the MORE is a photoelectrochemical device capable of delivering light via a fiber optic directly to the region of electrochemical measurement, allowing microelectrochemical study of systems with complex photochemistries. We have previously used MOREs with relatively thick rings (∼600 nm) to study the qualitative photoelectrochemistry of the dye methylene blue.[1] Results demonstrated that the MORE may be used to detect photoelectroactive species with lifetimes less than 90 μs.

Microring electrodes themselves find use in a wide range of electrochemical applications.[12−15] This is primarily because their large perimeter-to-area ratio results in an enhanced material flux to the electrode surface, leading to higher current densities and improved temporal resolution in the study of reactions with fast chemical and electrochemical kinetics. It is this temporal resolution that allows for the exploration of systems with fast photoelectrochemistries. However, for the MORE to be of any real quantitative utility, analytical expressions and/or numerical models are needed that relate the photocurrent to variables such as sensitizer concentration, light intensity, electrode dimensions, etc.

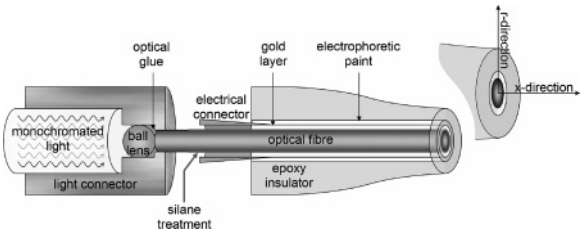

Figure 1. Schematic cross section of tip of MORE and homemade light coupling unit. Inset: the cylindrical polar geometry of the MORE problem, superimposed on the tip of the MORE.

Szabo[16] states that derivation of analytical expressions for the transport limited current to microrings in the dark is challenging because the diffusion equation must be solved subject to mixed boundary conditions where the flux is specified at one part of a surface and the concentration on another. Most (semi-)analytical approaches to solving the dark problem do so for so-called "thin rings" ((ring inner radius, a (m))/(outer radius, b (m)) > 0.91[16−19]), assuming a constant flux over the electrode surface. Exceptions are the work of Philips et al.,[20] Tallman et al.[21−24] and Wu et al.[25,26] More recently, Compton et al.[27] have,

* To whom all correspondence should be sent: Centre for Materials Science, University of Central Lancashire, Preston PR1 2HE, United Kingdom. Tel: +44 1772 893530. Fax: +44 01772 892996. E-mail: cboxall@uclan.ac.uk.

† Parts 1 and 2 presented in refs 1 and 2.

‡ University of Central Lancashire.

§ Imperial College.

10.1021/jp0622785 CCC: $33.50
Published on Web 07/27/2006

for the first time, used finite difference numerical methods to produce simulations for both chronoamperometry and linear sweep voltammetry at microrings of intermediate thickness.

Numerical simulations of the dark behavior of microrings notwithstanding, the availability of simple analytical solutions greatly facilitates the analysis of experimental data. Thus, we have recently derived analytical expressions for the steady-state transport limited photocurrent generated at MOREs with very thin rings ($a/b > 0.99$)[2] for two generic photoelectrochemical systems:

(i) A sensitizer, S, is photoexcited to form S* with quantum efficiency ϕ. This may then relax back to S (eq 1a) or be detected, e.g., oxidatively, at the electrode (a PE process, photophysical−electrochemical):

solution

$$S \xrightarrow{h\nu} S^* \xrightarrow{k_0} S \tag{1a}$$

electrode

$$S^* \rightarrow S^+ + e^-; \quad E^0_{S^*/S^+} \tag{1b}$$

(ii) Photoexcitation of S to S*, which may then relax back to S or undergo an electron-transfer process with a charge scavenger, A, to form S^+ and A^- (eq 1c). Either S^+ or A^- may then be detected at the electrode surface; for the purposes of this communication, we assume the photocurrent, i (A), is due to reduction of S^+, which may itself undergo some loss reaction (eq 1d) (a PCE process, photophysical−chemical−electrochemical):

solution

$$S^* + A \xrightarrow{k_1} S^+ + A^- \tag{1c}$$

solution

$$S^+ \xrightarrow{k_2} S \tag{1d}$$

electrode

$$S^+ + e^- \rightarrow S; \quad E^0_{S/S^+} \tag{1e}$$

where k_0 and k_2 are pseudo-first-order rate constants (s^{-1}) and k_1 is a second-order rate constant ($m^3\ mol^{-1}\ s^{-1}$).

In this paper we generate approximate analytical expressions for the time dependence of diffusion-limited photocurrents generated by these systems at very thin ring MOREs during light-on experiments. To test these expressions, it is necessary to construct very thin ring MOREs. Thus, this paper also describes the construction and photoelectrochemical characterization of very thin ring MOREs. These are then used to test the validity of our expressions using data from the $Ru(bipy)_3^{2+}$/Fe^{3+} PCE system.

2. Experimental Methods

MORE fabrication and dark electrochemical characterization, equipment, and optics (Figure 1) have been discussed elsewhere[1,28,29] and are described in detail in the Supporting Information (sections S1 and S2). All MOREs had gold rings with internal diameters of 250 μm and thicknesses of ~5 nm. All chemicals were of analytical grade or better. Distilled water, from a homemade still, was further purified by a deionization system (E pure model 04642, Barnstead/Thermodyne, Iowa, USA) to a resistivity of $1.8 \times 10^5\ \Omega$ m. Prior to electrochemical analysis, solutions were purged for 15 min with N_2 (white spot grade, BOC Ltd., Guildford, Surrey, U.K.) to remove dissolved O_2. All potentials were measured vs SCE.

3. Results and Discussion

3.1. Photoelectrochemical Characterization of MOREs. Let us now consider qualitative and quantitative photoelectrochemical characterization of very thin ring MOREs. A good model system for these purposes is the $Ru(bipy)_3^{2+}$/Fe^{3+} PCE system

$$Ru(bipy)_3^{2+} \underset{k_0}{\overset{h\nu,\phi}{\rightleftharpoons}} Ru(bipy)_3^{2+*} \tag{2a}$$

$$Ru(bipy)_3^{2+*} + Fe^{3+} \xrightarrow{k_1} [Ru(bipy)_3^{2+} \cdots Fe^{3+}]^* \xrightarrow{k'_1} Ru(bipy)_3^{3+} + Fe^{2+} \tag{2b}$$

$$[Ru(bipy)_3^{2+} \cdots Fe^{3+}]^* \xrightarrow{k_{-1}} Ru(bipy)_3^{2+} + Fe^{3+} \tag{2c}$$

$$Ru(bipy)_3^{3+} + Red \xrightarrow{k_2 = k'_2[Red]} Ru(bipy)_3^{2+} + Ox \tag{2d}$$

which has been discussed as a potential electrolyte for photogalvanic cells by Albery and Foulds.[30] Here $[Ru(bipy)_3^{2+} \cdots Fe^{3+}]^*$ indicates an imaginary cage, immediately leading to the alternative quenching routes of $Ru(bipy)_3^{2+*}$ described by k_1' (chemical quenching) and k_{-1} (physical quenching). Rate parameter k_2 describes the pseudo-first-order reduction of $Ru(bipy)_3^{3+}$ to $Ru(bipy)_3^{2+}$ by some reductant, Red (where $k_2 = k_2'[Red]$). The identity of reductant associated with eq 2d and this pseudo-first-order coefficient k_2 is addressed in section 3.4.

In chloride media, the iron couple behaves irreversibly. Thus, for a solution exclusively comprised of the starting reactants Fe^{3+} and $Ru(bipy)_3^{2+}$, no electrochemistry occurs in the dark between $E = +0.2$ V (onset of reduction of Fe(III) ($E^0(Fe^{3+}/Fe^{2+}) = 0.53$ V vs SCE)) and +1.03 V ($E^0(Ru(bipy)_3^{3+}/Ru(bipy)_3^{2+})$). However, under illumination $Ru(bipy)_3^{3+}$ and Fe^{2+} ions are generated (eq 2b). The reduction of photogenerated $Ru(bipy)_3^{3+}$ may occur at potentials $<\approx 0.9$ V. Further, due again to the aforementioned irreversibility of the iron couple, the oxidation of the concurrently photogenerated Fe^{2+} is only observed at potentials more positive than +0.6 V vs SCE. Thus, *under illumination*, there exists a potential window between +0.2 V (onset of Fe^{3+} reduction) and +0.6 V vs SCE (onset of Fe^{2+} oxidation) wherein the only electrochemistry that can occur within this system is the reduction of the photogenerated Ru(III) species, affording detection of a photocurrent derived from a single species ($Ru(bipy)_3^{3+}$). Following the methodology of Albery et al., we have used the MORE to measure photocurrents from a solution of 10 mM $Ru(bipy)_3^{2+}$, 5 mM Fe^{3+} at an applied potential of +0.5 V, as a function of irradiation wavelength, λ (nm or m). The results are shown in Figure 2, corrected for the transmittance of the ball lens and the incident light intensity at λ.

It can be seen from Figure 2 that the photocurrent action spectrum closely follows the form of the UV−visible absorption spectrum of $Ru(bipy)_3^{2+}$ in the wavelength range 350−700 nm, indicating that the observed photocurrent is due to the photoreduction of $Ru(bipy)_3^{3+}$ ions produced by the photoexcitation of $Ru(bipy)_3^{2+}$ ions followed by homogeneous solution-phase electron transfer to Fe^{3+} ions (eqs 2). Comparison of the form of the photocurrent spectrum with the UV−visible absorption spectrum allows for the photoelectrochemically active transition of $Ru(bipy)_3^{2+}$ to be assigned to the singlet-to-singlet, metal d

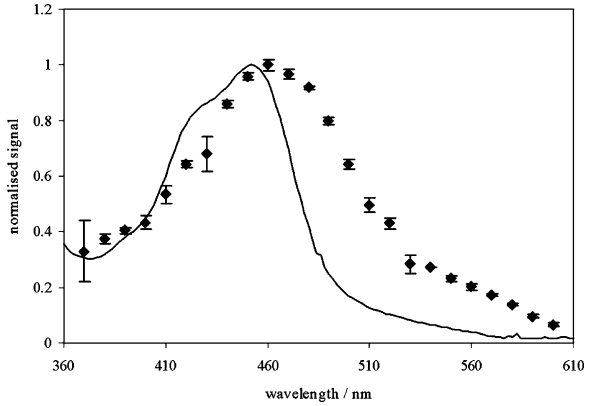

Figure 2. Comparison of (◆) normalized photocurrent action spectrum recorded using a MORE at $E = +0.5$ V vs SCE from a pH 2 solution containing 10 mol m^{-3} $Ru(bipy)_3Cl_2$, 5 mol m^{-3} $FeCl_3$, with (—) normalized UV−visible absorption spectrum of $Ru(bipy)_3^{2+}$.

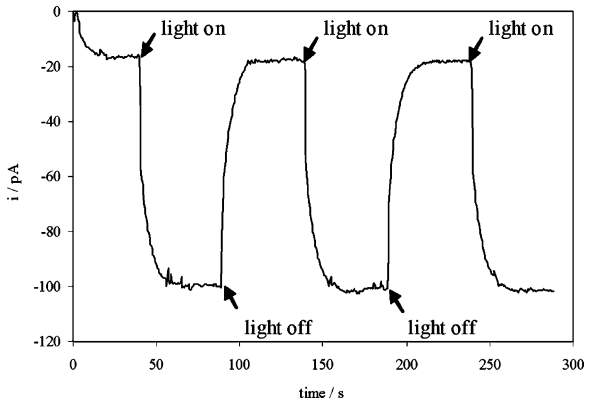

Figure 3. Transient chronoamperogram of a solution of 10 mol m^{-3} $Ru(bipy)_3Cl_2$ and 5 mol m^{-3} $FeCl_3$ recorded at the MORE while switching the light on and off. $\lambda = 460$ nm, $E = +0.5$ V vs SCE, pH = 2.

orbital-to-ligand π^*-antibonding orbital charge-transfer band.[31,32] Figure 2 also indicates that the MORE could be used as a selective photoelectroanalytical tool, capable of differentiating between two or more photoactive species provided their λ_{max} values are sufficiently separated.

We have also examined the reproducibility and time dependence of the photocurrents shown in Figure 2. Figure 3 shows the light on/light off photocurrent transients recorded at $\lambda =$ 460 nm. The cathodic photocurrent due to the reduction of photogenerated $Ru(bipy)_3^{3+}$ exhibits reproducibility in terms of both magnitude and form, suggesting that the data may be of a quality to yield useful information upon quantitative analysis. Analysis of the magnitude and form of the photochronoamperometric transient is the subject of the next section.

3.2. Theory for the Diffusion-Limited, Light-On, Transient Photocurrent from a PE System. The system to be modeled is shown in eqs 1a and 1b. An expression that describes the diffusion-limited, light-on transient photocurrent generated by this system can be derived by using the cylindrical polar coordinate system shown in the inset of Figure 1, wherein x (m) is the distance into solution from and normal to the plane of the electrode surface and r (m) the radial distance from the center of the optical disk. The disk is assumed to be uniformly illuminated by parallel light, switched on at time $t = 0$ (s), passing from the disk into solution (the validity of this assumption has been discussed previously[2]). Using a similar approach to that employed when we modeled the steady-state behavior of the MORE,[2] the time dependent diffusion equation for S* is set up using the following assumptions:

1.1. The light makes only a small perturbation to [S], thus not altering significantly any current associated with its dark oxidation or reduction, upon which the photocurrent may be superimposed. This also means that the solution does not bleach and that the light has a Beer−Lambert profile given by $I = I_{ph}e^{-\epsilon_\lambda[S]x}$, where I ((mol photons) m^{-2} s^{-1}) is the flux of light at distance x.

1.2. The homogeneous loss reaction is pseudo-first-order with respect to [S*] with rate coefficient k_0.

1.3. The electron transfer kinetics of S* at the electrode when the ring is switched on are extremely rapid, the photocurrent being under either mass transport or photochemical kinetic control.

In analogy to the steady-state problem[2] and using the following dimensionless variables

$$\chi = \frac{x}{X_{k,0}} \tag{3a}$$

$$\rho = \frac{r}{X_{k,0}} \tag{3b}$$

$$U = \frac{D_S[S^*]}{\phi' I_{ph} X_\epsilon} \tag{3c}$$

$$\gamma = \frac{X_{k,0}}{X_\epsilon} \tag{3d}$$

$$\tau = k_0 t \tag{3e}$$

where D_S is the diffusion coefficient (m^2 s^{-1}) of S of concentration [S] (mol m^{-3}), I_{ph} is the flux of light at the electrode surface ((mol photons) m^{-2} s^{-1}), ϵ_λ is the absorption coefficient (m^2 mol^{-1}) at λ, and all other symbols take their usual meaning. The time dependent diffusion equation for S* in cylindrical polar coordinates can be written as follows

at $\rho < \rho_0$

$$\frac{\partial U}{\partial \tau} = \frac{\partial^2 U}{\partial \rho^2} + \frac{1}{\rho}\frac{\partial U}{\partial \rho} + \frac{\partial^2 U}{\partial \chi^2} - U + \gamma^2 e^{-\gamma\chi} \tag{4a}$$

and at $\rho > \rho_0$

$$\frac{\partial U}{\partial \tau} = \frac{\partial^2 U}{\partial \rho^2} + \frac{1}{\rho}\frac{\partial U}{\partial \rho} + \frac{\partial^2 U}{\partial \chi^2} - U \tag{4b}$$

inside and outside the beam, respectively. ρ_0 and ρ_1 are the normalized inner and outer radii of the ring where

$$\rho_o = a/X_{k,0}, \quad \rho_1 = b/X_{k,0} \tag{5a,b}$$

and

$$X_{k,0} = (D_S/k_0)^{1/2} \tag{6a}$$

the thickness of the reaction layer and

$$X_\epsilon = (\epsilon_\lambda[S])^{-1} \tag{6b}$$

the thickness of the absorbance layer.

For the PE system described by eqs 1, at $\tau = 0$, $U = 0$ for all χ and ρ. If it is further assumed that I is invariant with x as

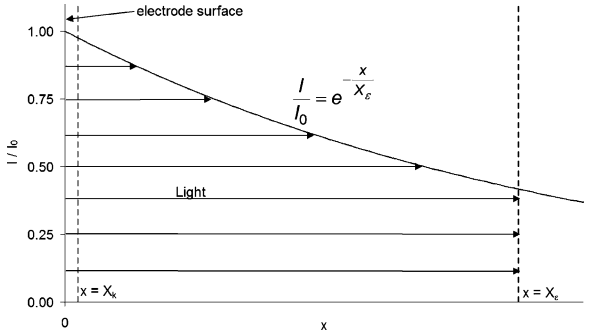

Figure 4. Beer−Lambert profile perpendicular to the surface of the MORE, showing the relative thicknesses of $X_{k,0}$ and X_ϵ as required by eq 7.

a result of low [S] and/or low ϵ_λ, then Laplace transformation of eqs 6 gives

$$\frac{\partial^2\bar{U}}{\partial\rho^2}+\frac{1}{\rho}\frac{\partial\bar{U}}{\partial\rho}+\frac{\partial^2\bar{U}}{\partial\chi^2}-(s+1)\bar{U}+\frac{\gamma^2}{s}=0 \qquad (7a)$$

$$\frac{\partial^2\bar{U}}{\partial\rho^2}+\frac{1}{\rho}\frac{\partial\bar{U}}{\partial\rho}+\frac{\partial^2\bar{U}}{\partial\chi^2}-(s+1)\bar{U}=0 \qquad (7b)$$

inside and outside the beam, respectively. The approximation underlying the derivation of eq 7 from eq 6 implies that $X_{k,0} < X_\epsilon$, the resultant relative thicknesses of both layers being illustrated in Figure 4.

We are investigating a diffusion transport-limited oxidation process given in eq 1b. Thus, the normalized Laplace transformed boundary conditions for the solution of eqs 7 are given in Table 1. Following our previous approach, it is instructive to consider the time dependence of the concentration field generated at the MORE when the microring is switched OFF, i.e., there is no electrochemistry occurring at the surface, whereupon eqs 7a and 7b reduce respectively to

$$\frac{\partial^2\bar{U}}{\partial\rho^2}+\frac{1}{\rho}\frac{\partial\bar{U}}{\partial\rho}-(s+1)\bar{U}+\frac{\gamma^2}{s}=0 \qquad (8a)$$

$$\frac{\partial^2\bar{U}}{\partial\rho^2}+\frac{1}{\rho}\frac{\partial\bar{U}}{\partial\rho}-(s+1)\bar{U}=0 \qquad (8b)$$

Again, by analogy with the steady-state problem,[2] noting that eqs 8 have the form of Bessel's modified equation and through application of boundary condition B4, the following can be shown:

at $\rho < \rho_0$, ring off:

$$\bar{U}_{\text{inside}}=\frac{\gamma^2}{s(s+1)}[1-\sqrt{s+1}\rho_o K_1(\sqrt{s+1}\rho_o)I_o(\sqrt{s+1}\rho)] \qquad (9a)$$

at $\rho > \rho_0$, ring off:

$$\bar{U}_{\text{outside}}=\frac{\gamma^2}{s(s+1)}[\sqrt{s+1}\rho_0 I_1(\sqrt{s+1}\rho_0)K_0(\sqrt{s+1}\rho)] \qquad (9b)$$

where $I_m(z)$ and $K_m(z)$ are modified Bessel functions of the first and second kinds, respectively, order m. We will return to this result below.

We now consider the concentration field generated at the MORE when the ring is switched ON; i.e., S* is consumed at the electrode surface under diffusion control. Similar to the steady-state problem (to which the interested reader should refer for more detail regarding the following derivation[2]), this requires the solution of eq 7b using a discontinuous boundary condition—in this instance, boundary condition B6. The resultant solution matching through boundary condition B4 at $\rho = \rho_0$ produces a set of dual integral equations that are analytically intractable. However, this difficulty can be obviated by assuming that eq 7a applies in the range $0 < \rho < \rho_1$ rather than $0 < \rho < \rho_0$, i.e., that it applies over the ring, even though no photogeneration occurs in that space. We have shown that this approximation holds for very thin rings where $\rho_0/\rho_1 > 0.99$, with a resultant error in the calculated S* concentration field of less than 5.1% if $\rho_0 < 20$.[2] With these restrictions in mind then, by analogy with the steady-state problem and through application of boundary condition B6b at $\rho < \rho_0$, it can be shown that the general solution of eq 7a is of the form

$$\bar{U}=\frac{\gamma^2}{s(s+1)}+CI_0(\sqrt{s+1}\rho)+C'\int_0^\infty f(\lambda)J_0(\lambda\rho)e^{-(s+1+\lambda^2)^{1/2}\chi}\,d\lambda \qquad (10)$$

where C and C' are arbitrary constants of integration, λ is an arbitrary real nonzero constant, and $J_m(z)$ is a Bessel function of the first kind, order m. Function $f(\lambda)$ can be determined by application of discontinuous boundary condition B6 at $\rho = \rho_0$. C' can be determined by application of condition B6a at $\chi = 0$, $\rho = \rho_0$. Finally, concentration and concentration gradient matching at the beam surface (boundary condition B4) at $\chi \rightarrow \infty$ allows for the determination of C giving, at $\rho < \rho_1$ when the ring is ON

$$\bar{U}=\frac{\gamma^2}{s(s+1)}\left\{1-\sqrt{s+1}\rho_0K_1(\sqrt{s+1}\rho_0)I_0(\sqrt{s+1}\rho)-(1-\sqrt{s+1}\rho_0K_1(\sqrt{s+1}\rho_0)I_0(\sqrt{s+1}\rho_0))\frac{\int_0^\infty\frac{\cos(\rho_0\lambda)}{\sqrt{s+1+\lambda^2}}J_0(\lambda\rho)e^{-(s+1+\lambda^2)^{1/2}\chi}\,d\lambda}{\int_0^\infty\frac{\cos(\rho_0\lambda)}{\sqrt{s+1+\lambda^2}}J_0(\lambda\rho_0)\,d\lambda}\right\} \qquad (11)$$

Substitution of eq 11 into 7a confirms that it is a solution of that equation. Reverse transformation of eq 11 is impossible. However, we are concerned with the time dependence of the light-on photocurrent. Differentiation of eq 11 with respect to χ then gives, at the electrode surface $\chi = 0$

$$\left(\frac{\partial\bar{U}}{\partial\chi}\right)_{\chi=0}=\frac{\gamma^2}{s(s+1)}\left[(1-\sqrt{s+1}\rho_0K_1(\sqrt{s+1}\rho_o)I_0(\sqrt{s+1}\rho_0))\frac{\int_0^\infty\cos(\rho_0\lambda)J_0(\lambda\rho)\,d\lambda}{\int_0^\infty\frac{\cos(\rho_0\lambda)}{\sqrt{s+1+\lambda^2}}J_0(\lambda\rho_0)\,d\lambda}\right] \qquad (12)$$

TABLE 1: Laplace Transformed Boundary Conditions for the Solution of Eqs 9

$\bar{U}$ is finite over all space	(B1)
when $\rho \rightarrow \infty$ and $0 < \chi < \infty$ $(\partial\bar{U}/\partial\rho)_{\rho\rightarrow\infty} \rightarrow 0$; $\bar{U} \rightarrow 0$	(B2)
at $\chi \rightarrow \infty$ and $0 < \rho < \infty$ $(\partial\bar{U}\partial\chi)_{\chi\rightarrow\infty} = 0$	(B3)
at $\rho = \rho_0$ $\bar{U}_{\text{insidebeam}} = \bar{U}_{\text{outsidebeam}}$ & $(\partial\bar{U}/\partial\rho)_{\text{insidebeam}} = (\partial\bar{U}/\partial\rho)_{\text{outsidebeam}}$	(B4)
when ring is switched off, i.e., no electrochemistry at electrode surface	
at $\chi = 0$ and for $0 < \rho < \infty$ $(\partial\bar{U}/\partial\chi)_{\chi=0} = 0$	(B5)
when ring is switched on	
at $\chi = 0$ and $\rho_0 < \rho < \rho_1$ $(\partial\bar{U}/\partial\chi)_{\chi=0} \neq 0$; $\bar{U} = 0$ and	(B6a)
at $\chi = 0$ and $0 < \rho < \rho_0$ & $\rho_1 < \rho < \infty$ $(\partial\bar{U}/\partial\chi)_{\chi=0} = 0$	(B6b)

which, at large $\sqrt{s+1}\,\rho_0$ (short time and/or large disk) can be shown to simplify to (section S3 in Supporting Information)

$$\left(\frac{\partial\bar{U}}{\partial\chi}\right)_{\chi=0} = \frac{\gamma^2\sqrt{\rho_0}}{2.14\sqrt{\rho^2-\rho_0{}^2}}\frac{1}{s(s+1)^{2/3}} \tag{13}$$

By applying the convolution theorem,[33] it can be shown that (section S4 in Supporting Information)

$$L^{-1}\left\{\frac{1}{s(s+1)^{2/3}}\right\} = \frac{1}{\Gamma(2/3)}\int_0^\tau y^{-1/3}\,\mathrm{e}^{-y}\,\mathrm{d}y = \frac{3}{2\Gamma(2/3)}\int_0^{\tau^{2/3}}\mathrm{e}^{-z^{3/2}}\,\mathrm{d}z \tag{14}$$

where

$$z = y^{2/3}$$

Using the identity given by eq 14, the reverse transform of eq 13 may then be given as

$$\left(\frac{\partial U}{\partial\chi}\right)_{\chi=0} = \frac{\gamma^2\sqrt{\rho_0}}{2.14\sqrt{\rho^2-\rho_0{}^2}}\frac{3}{2\Gamma(2/3)}\int_0^{\tau^{2/3}}\mathrm{e}^{-z^{3/2}}\,\mathrm{d}z \tag{15}$$

According to Fick's first law, the photocurrent obtained through the ring is given by

$$\frac{i}{nFD_{\mathrm{S}}} = 2\pi\int_a^b\left(\frac{\partial[\mathrm{S}^*]}{\partial x}\right)_{x=0} r\,\mathrm{d}r \tag{16}$$

Recasting eq 15 in terms of the original variables and substituting into eq 16 gives

$$\frac{i}{i_{t\rightarrow\infty}} = \frac{3}{2\Gamma(2/3)}\int_0^{(k_0t)^{2/3}}\mathrm{e}^{-z^{3/2}}\,\mathrm{d}z \tag{17}$$

$$i_{t\rightarrow\infty} = \frac{\pi nFD_{\mathrm{S}}\phi I_{\mathrm{ph}}\epsilon_\lambda[\mathrm{S}]}{1.07k_0}\sqrt{\frac{a}{X_{k,0}}}\sqrt{b^2-a^2} = \frac{\pi nFD_{\mathrm{S}}{}^{3/4}a^{1/2}I_{\mathrm{ph}}\epsilon_\lambda[\mathrm{S}]\sqrt{b^2-a^2}}{1.07}\left(\frac{\phi}{k_0{}^{3/4}}\right) \tag{18}$$

Equation 18 has the form of the steady state solution that we obtained previously (eq 22 in ref 2), confirming the internal consistency of our approach. Figure 5 shows the time dependence of the photocurrent, calculated from eq 17 and further normalized with respect to $k_0{}^{3/4}$, as a function of k_0. As might be expected, the larger k_0, (i) the lower the steady-state photocurrent and (ii) the shorter the time to steady state. k_0 can be obtained by curve fitting normalized experimental light-on photocurrent data to eq 17. Assuming all preparenthetical terms in eq 18 are known, then use of this value of k_0, in conjuction with $i_{t\rightarrow\infty}$ data and eq 18 allows for calculation of ϕ. Thus, the measurement of one simple photocurrent light-on transient allows for the complete characterization of a PE system. Having shown that the MORE can be used to characterize PE systems, let us now consider the behavior of PCE systems.

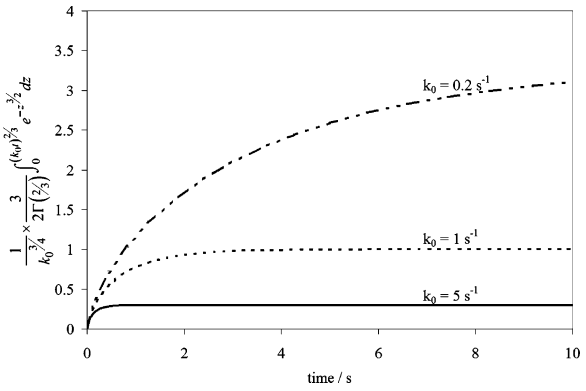

Figure 5. The normalized, theoretical, mass-transport limited, light on transient photocurrent, $(i/(i_{t\rightarrow\infty}k_0{}^{3/4}))$, at a MORE for a PE system at a range of k_0 values.

3.3. Theory for the Diffusion-Limited, Light-On, Transient Photocurrent from a PCE System. The system to be modeled is given in eqs 1a and 1c−1e. As in section 3.2, the time-dependent diffusion equations for S* and S^+ (the latter being the species that is detected at the electrode surface) are set up using assumptions 1.1−1.3, as well as assumptions 2.1−2.3 below:

2.1. the loss reaction, eq 1d, is pseudo-first-order with respect to $[S^+]$ with rate coefficient k_2.

2.2. A is in such excess that (a) [A] is uniform in the vicinity of S/S* and the electron-transfer reaction (eq 1c) is pseudo-first-order with respect to [S*], i.e., either [S], ϕ, or I_{ph} is small and so k_1[A] can be considered constant; (b) the kinetics of electron transfer between S* and A are fast compared to those of mass transport of S*. Thus A reacts with S* before S* diffuses any significant distance

2.3. The electron-transfer kinetics of S^+ at the electrode are extremely rapid, so the photocurrent is under either mass transport or photochemical kinetic control.

The coupled diffusion equations for S* and S^+ inside the beam are then given by

$$\frac{\partial[\mathrm{S}^*]}{\partial t} = D_{\mathrm{S}}\frac{\partial^2[\mathrm{S}^*]}{\partial x^2} + D_{\mathrm{S}}\frac{\partial^2[\mathrm{S}^*]}{\partial r^2} + \frac{D_{\mathrm{S}}}{r}\frac{\partial[\mathrm{S}^*]}{\partial r} - (k_0 + k_1[\mathrm{A}])[\mathrm{S}^*] + \phi I_{\mathrm{ph}}\epsilon_\lambda[\mathrm{S}]\,\mathrm{e}^{-\epsilon_\lambda[\mathrm{S}]x} \tag{19a}$$

$$\frac{\partial[\mathrm{S}^+]}{\partial t} = D_{\mathrm{S}}\frac{\partial^2[\mathrm{S}^+]}{\partial x^2} + D_{\mathrm{S}}\frac{\partial^2[\mathrm{S}^+]}{\partial r^2} + \frac{D_{\mathrm{S}}}{r}\frac{\partial[\mathrm{S}^+]}{\partial r} - k_2[\mathrm{S}^+] + k_1[\mathrm{A}][\mathrm{S}^*] \tag{19b}$$

From assumption 2.2, terms that refer to diffusion in eq 19a may be neglected. As in the PE case, when $t = 0$, $S^* = 0$ for all x and r. Using this boundary condition, eq 19a may be solved to give an expression for S* which, upon substitution into eq 19b gives

$$\frac{\partial[S^+]}{\partial t} = D_S\frac{\partial^2[S^+]}{\partial x^2} + D_S\frac{\partial^2[S^+]}{\partial r^2} + \frac{D_S}{r}\frac{\partial[S^+]}{\partial r} - k_2[S^+] + \frac{k_1[A]}{(k_0 + k_1[A])}\phi I_{ph}\epsilon_\lambda[S]\, e^{-\epsilon_\lambda[S]x}(1 - e^{-(k_0+k_1[A])t}) \quad (20)$$

Equation 20 may be recast in a nondimensionalized form analogous to that of eq 4a except that expressions for χ, ρ, and U (eqs 3) are now written in terms of k_2, $X_{k,2}$, ϕ', and S^+ where

$$\phi' = \phi\frac{k_1[A]}{k_0 + k_1[A]} \quad (21)$$

If, as in the PE case, it is assumed that I is invariant with x, then Laplace transformation of the nondimensional form of eq 20 gives that, inside and outside the beam, respectively

$$\frac{\partial^2\bar{U}}{\partial\rho^2} + \frac{1}{\rho}\frac{\partial\bar{U}}{\partial\rho} + \frac{\partial^2\bar{U}}{\partial\chi^2} - (s+1)\bar{U} + \frac{\gamma'^2}{s} = 0 \quad (22a)$$

$$\frac{\partial^2\bar{U}}{\partial\rho^2} + \frac{1}{\rho}\frac{\partial\bar{U}}{\partial\rho} + \frac{\partial^2\bar{U}}{\partial\chi^2} - (s+1)\bar{U} = 0 \quad (22b)$$

where

$$\gamma'^2 = \gamma^2\frac{\beta}{s+\beta} \quad \text{and} \quad \beta = \frac{k_0 + k_1[A]}{k_2} \quad (23a,b)$$

Equations 22 are analogous to eqs 7 with γ' replacing γ. Further, the boundary conditions of Table 1 also apply to eq 22, even though U, ρ, and χ are now written in terms of k_2, S^+, and ϕ'. Consequently, the algebraic manipulations of eqs 7 given by eqs 8−11 are directly applicable to eqs 22, allowing us to deduce (upon substitution of γ' through eq 22a) that, when the electrochemical microring is OFF

at $\rho < \rho_0$:

$$\bar{U}_{inside} = \frac{\gamma^2\beta}{s(s+1)(s+\beta)}[1 - \sqrt{s+1}\rho_0 K_1(\sqrt{s+1}\rho_0)I_0(\sqrt{s+1}\rho)] \quad (24a)$$

at $\rho > \rho_0$:

$$\bar{U}_{outside} = \frac{\gamma^2\beta}{s(s+1)(s+\beta)}[\sqrt{s+1}\rho_0 I_1(\sqrt{s+1}\rho_0)K_0(\sqrt{s+1}\rho)] \quad (24b)$$

and that when the ring is switched ON at $\rho_1 > \rho > 0$

$$\bar{U} = \frac{\gamma^2\beta}{s(s+1)(s+\beta)}\left\{1 - \sqrt{s+1}\rho_0 K_1(\sqrt{s+1}\rho_0)I_0(\sqrt{s+1}\rho) - (1 - \sqrt{s+1}\rho_0 K_1(\sqrt{s+1}\rho_0)I_0(\sqrt{s+1}\rho_0))\frac{\int_0^\infty \frac{\cos(\rho_0\lambda)}{\sqrt{s+1+\lambda^2}} J_0(\lambda\rho)\, e^{-(s+1+\lambda^2)^{1/2}\chi}\, d\lambda}{\int_0^\infty \frac{\cos(\rho_0\lambda)}{\sqrt{s+1+\lambda^2}} J_0(\lambda\rho_0)\, d\lambda}\right\} \quad (25)$$

Again, we are interested in the light-on transient photocurrent. By following the method of eqs 11−13

$$\left(\frac{\partial\bar{U}}{\partial\chi}\right)_{\chi=0} = \frac{\gamma^2\sqrt{\rho_0}}{2.14\sqrt{\rho^2 - \rho_0^2}}\frac{\beta}{s(s+\beta)(s+1)^{2/3}} \quad (26)$$

By use of partial fractions and convolution theorem, it can be shown that[33]

$$\left(\frac{\partial U}{\partial\chi}\right)_{\chi=0} = \frac{\gamma^2\sqrt{\rho_0}}{2.14\sqrt{\rho^2 - \rho_0^2}}\frac{3}{2\Gamma(2/3)}\left(\int_0^{\tau^{2/3}} e^{-z^{3/2}}\, dz - e^{-\beta\tau}\int_0^{\tau^{2/3}} e^{-(1-\beta)z^{3/2}}\, dz\right) \quad (27)$$

Treating eq 27 in a manner analogous to eqs 15−18 allows the derivation of eqs 28 and 29

$$\frac{i}{i_{t\to\infty}} = \frac{3}{2\Gamma(2/3)}\left(\int_0^{\tau^{2/3}} e^{-z^{3/2}}\, dz - e^{-\beta\tau}\int_0^{\tau^{2/3}} e^{-(1-\beta)z^{3/2}}\, dz\right) \quad (28)$$

$$\frac{1}{i_{t\to\infty}} = \left(\frac{\pi nFD_S^{3/4}a^{1/2}I_{ph}\epsilon_\lambda[S]\sqrt{b^2 - a^2}}{1.07}\right)^{-1}\left(\frac{\phi}{k_2^{3/4}}\right)^{-1}\left(1 + \frac{k_0}{k_1[A]}\right) \quad (29)$$

Figure 6 shows the normalized photocurrent as a function of τ and β calculated from eq 28. To facilitate the extraction of useful kinetic information from experimental data, we use eqs 26 and 27 to identify simpler, asymptotic solutions. For large β ($\beta > s$, $\beta > 1$), both eqs 26 and 27 reduce to

$$\frac{i}{i_{t\to\infty}} = \frac{3}{2\Gamma(2/3)}\left(\int_0^{\tau^{2/3}} e^{-z^{3/2}}\, dz\right) = \frac{3}{2\Gamma(2/3)}\left(\int_0^{(k_2t)^{2/3}} e^{-z^{3/2}}\, dz\right) \quad (30a)$$

For small β ($\beta < 1$), eq 27 reduces to

$$\frac{i}{i_{t\to\infty}} = \frac{3}{2\Gamma(2/3)}(1 - e^{-\beta\tau})\left(\int_0^{\tau^{2/3}} e^{-z^{3/2}}\, dz\right) = \frac{3}{2\Gamma(2/3)}(1 - e^{-(k_0+k_1[A])t})\left(\int_0^{(k_2t)^{2/3}} e^{-z^{3/2}}\, dz\right) \quad (30b)$$

Equation 30a describes the case where electron transfer between S* and A, and so generation of S^+ is fast on the time scale of the light-on transient experiment, i.e., $k_1[A]$ is large: thus the form of the photocurrent transient for the PCE system is largely determined by the back reaction of S^+ to S. In this way, it is analogous to the PE system where the form of the

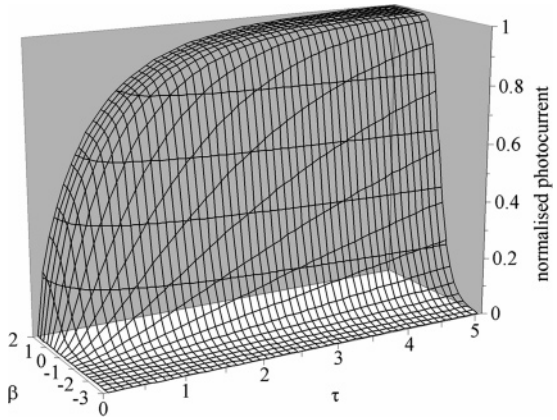

Figure 6. The normalized, theoretical, mass-transport limited, light on transient photocurrent at a MORE for a PCE system as a function of τ ($= k_2t$) at a range of β ($=(k_0 + k_1[A])/k_2$) from eq 28.

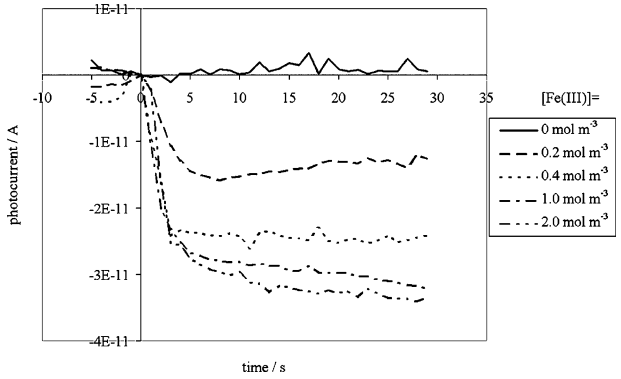

Figure 7. Light-on (at $t = 0$) photocurrent transients recorded using a very thin ring MORE ($a/b > 0.999$) for $[Ru(bipy)_3^{2+}] = 2$ mol m^{-3} and $[Fe^{3+}] = 0.2, 0.4, 1, 2$, mol m^{-3}. $\lambda = 460$ nm; $E = 0.5$ V; pH $=$ 2.

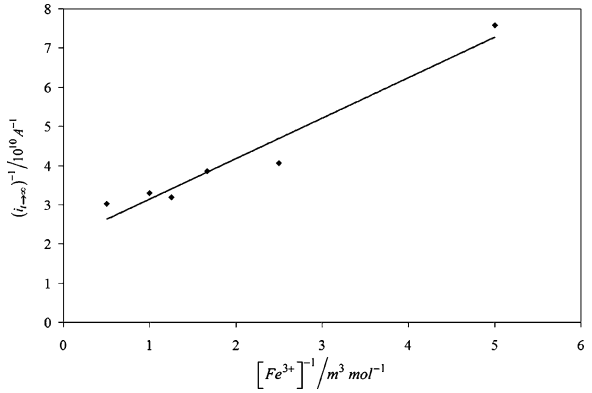

Figure 8. Reciprocal photocurrents observed from the $Ru(bipy)_3^{2+}$/Fe^{3+} system at a very thin ring MORE ($a/b > 0.999$) as a function of $[Fe^{3+}]^{-1}$. $[Ru(bipy)_3^{2+}] = 2$ mol m^{-3}; $\lambda = 460$ nm; $E = 0.5$ V; $\epsilon_{460} =$ 1382.5 m^2 mol^{-1}; pH $= 2$; minimum signal to noise ratio of source photocurrent data $= 15$.

light on transient is also determined by the relaxation of the electrochemically detected species to its ground state, i.e., S* to S through k_0. Equation 30b describes the case where generation of S^+ is slow on the time scale of the transient experiment. In this instance, the time dependence of the photocurrent signal is determined by not only the loss of S^+ but also the rate of generation of S^+, explicitly described by the factor $(1 - e^{-\beta\tau})$ in eq 30b.

For ease of analysis of experimental data, it is suggested that photocurrent transients are recorded under conditions of large [A], large β, where eq 30a obtains, rather than the more

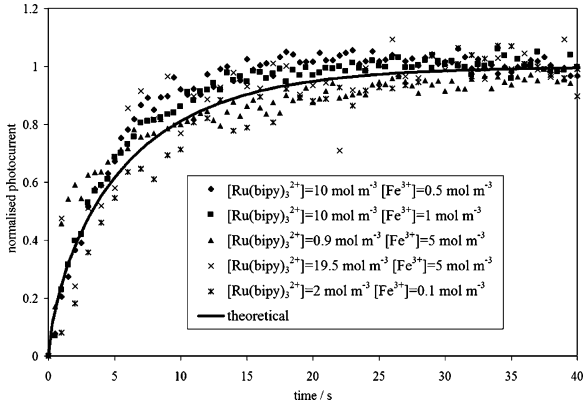

Figure 9. Normalized experimental photocurrent data of Figure 7, overlaid with theoretical light-on photocurrent transient, calculated using eq 30a and $k_2 = 0.115$ s^{-1}.

complicated eq 30b. Curve fitting of eq 30a to the experimental data then allows for the extraction of a value of k_2. Steady-state photocurrent values, recorded over all [A] may then be used to construct a $(i_{t\to\infty})^{-1}$ vs $[A]^{-1}$ plot in accordance with eq 29. This should yield a straight line with a (slope/intercept) value equal to k_0/k_1, which in turn corresponds to $1/K_{SV}$, the reciprocal Stern−Volmer coefficient for the system. Assuming that the values of all terms in the first set of parentheses of eq 29 are known, then in conjunction with the value of k_2 obtained from the transient data, ϕ may be obtained from eq 29 and the value of the intercept of the $(i_{t\to\infty})^{-1}$ vs $[A]^{-1}$ plot. Alternatively, given that, from eq 29, $i_{t\to\infty} \propto [S]$, ϕ may also be obtained from the slope of an $i_{t\to\infty}$ vs [S] plot for data recorded at constant [A], various [S].

3.4. Photoelectrochemical Studies of the $Ru(bipy)_3^{2+}$/Fe^{3+} System. Having modeled the light-on transient photocurrents for both PE and PCE systems at the MORE, let us consider the application of these models to the $Ru(bipy)_3^{2+}$/Fe^{3+} PCE system of eqs 2. Because of the explicit involvement of an imaginary cage in eqs 2b and 2c, eq 29 must be slightly rewritten in order to account for the efficiency, ϕ_{CE}, of the primary redox products $Ru(bipy)_3^{3+}$ and Fe^{2+} escaping the cage recombination reaction given by eq 2c

$$\frac{1}{i_{t\to\infty}} = \left(\frac{\pi nFD_{Ru}{}^{3/4}a^{1/2}I_{ph}\epsilon_\lambda[Ru(bipy)_3{}^{2+}]\sqrt{b^2-a^2}}{1.07}\right)^{-1} \left(\frac{\phi_{CE}\phi}{k_2{}^{3/4}}\right)^{-1}\left(1+\frac{k_0}{k_1[A]}\right) \quad (31)$$

where D_{Ru} is the diffusion coefficient of $Ru(bipy)_3^{2+}$ and all other symbols take their usual meanings. Figure 7 shows a family of light-on current transients recorded at constant $[Ru(bipy)_3^{2+}]$ and various $[Fe^{3+}]$.

Figure 8 shows the reciprocal steady-state photocurrents plotted vs $[Fe^{3+}]^{-1}$ in accordance with eq 31. Good linearity is observed, giving $k_1/k_0 = K_{SV} = 2.05$ m^3 mol^{-1}, which is in good agreement with a literature values of 0.9−1.6 m^3 mol^{-1} [32] derived by spectrofluorimetric measurements. Such measurements give a lifetime of the emitting state of $Ru(bipy)_3^{2+}$* of 610 ns,[34,35] allowing derivation of a value of $k_0 = 1.64 \times 10^6$ s^{-1} and, from $K_{SV} = 2.05$ m^3 mol^{-1}, $k_1 = 3.36 \times 10^6$ m^3 mol^{-1} s^{-1}. This compares well with a literature k_1 of 2.6×10^6 m^3 mol^{-1} s^{-1}.[32]

Returning to the time dependence of the photocurrent, eq 30a indicates that, as long as $(k_0 + k_1[A]) > k_2$, the transient curves

TABLE 2: Values for Kinetic Parameters Obtained Using the MORE

parameter	calculated value	lit. value	ref
$K_{SV} = k_1/k_0$	2.05 $m^3\ mol^{-1}$	0.9−1.6 $m^3\ mol^{-1}$	32
k_0		$1.64 \times 10^6\ s^{-1}$	32, 34, 35
k_1	$3.36 \times 10^6\ m^3\ mol^{-1}\ s^{-1}$	$2.6 \times 10^6\ m^3\ mol^{-1}\ s^{-1}$	32
k_2	$0.115\ s^{-1}$		
ϕ		1.07	35
ϕ_{CE}	0.099		
k'_1/k_{-1}	0.11 (average)		

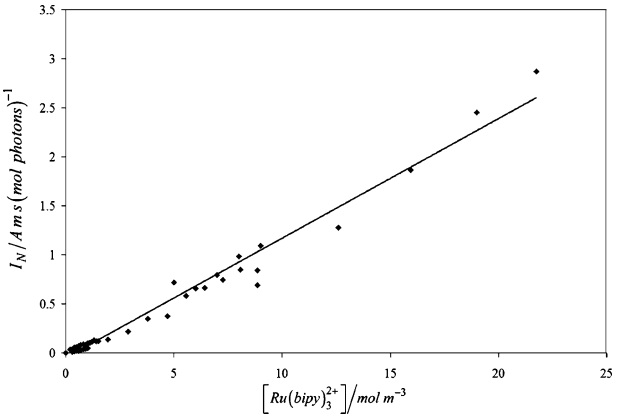

Figure 10. Normalized photocurrent, I_N, vs $[Ru(bipy)_3^{2+}]$ for $Ru(bipy)_3^{2+}/Fe^{3+}$ system (five datasets) at very thin ring MOREs. $I_N = i_{t\to\infty}(1 + (K_{SV}[Fe^{3+}])^{-1})/(I_{ph}(b^2 - a^2)^{1/2})$ (see text). pH = 2; λ = 460 nm; E = 0.5 V; a = 125 μm; $\epsilon_{460} = 1382.5\ m^2\ mol^{-1}$. Minimum sinal to noise (S/N) ratio of source data = 2. Data with $S/N < 2$ discarded. 83% of data have $S/N > 5$.

of Figure 7 should normalize onto a common curve, from which a value of k_2 may be obtained by fitting to eq 30a. Figure 9 confirms these expectations, with all normalized i vs t traces being fitted using eq 30a and $k_2 = 0.115\ s^{-1}$. The identity of reductant associated with eq 2d and this pseudo-first-order coefficient k_2 is discussed in the Supporting Information (section S5). Rate coefficients measured using the MORE and their available literature values are summarized in Table 2, from which it can be seen that the assumption underlying the use of eq 30a is satisfied, i.e., that $(k_0 + k_1[A]) > k_2$.

Knowing k_0/k_1 and k_2, it can be seen from eq 31 that it is possible to calculate $\phi\phi_{CE}$ from the intercept of Figure 8. From that intercept of $2.12 \times 10^{-10}\ A^{-1}$, and values of D_{Ru}, I_{ph}, and $(b^2 - a^2)^{1/2}$ of $2.8 \times 10^{-10}\ m^2\ s^{-1}$,[36] 2.6×10^{-4} (mol photons) $m^{-2}\ s^{-1}$, and $4.5 \times 10^{-7}\ m^2$, respectively, a value of $\phi\phi_{CE} = 0.13$ may be obtained. However, $\phi\phi_{CE}$ may also be obtained from a second MORE experiment.

Figure 10 shows the results of five experiments wherein the steady-state photocurrent is measured as a function of $[Ru(bipy)_3^{2+}]$. To allow for experiment-to-experiment variations in $[Fe^{3+}]$ and specific MORE used, the photocurrents have been normalized with respect to I_{ph}, $(b^2 - a^2)^{1/2}$ and $(1 + (K_{SV}[Fe^{3+}])^{-1})^{-1}$ (using the K_{SV} value determined from Figure 8). Equation 31 predicts that $i \propto [Ru(bipy)_3^{2+}]$. Figure 10 confirms that this is the case. Again, knowing k_1/k_0 and k_2 and all other experimental parameters, it is possible, by use of eq 31, to extract from the slope of Figure 10 a value of $\phi\phi_{CE}$ which, for these data, is found to be 0.081. This compares well with the value of 0.13 obtained from Figure 8 above.

Parameter ϕ is the quantum efficiency for the formation of the triplet $Ru(bipy)_3^{2+}*$ species, for which a value of 1.07 has been obtained by transient spectroscopic methods.[35] This allows calculation of $\phi_{CE} = 0.12$ (Figure 8 data) and 0.076 (Figure 10 data), average = 0.099, a value that compares well with that of $\phi_{CE} = 0.11$ for the $Ru(bipy)_3^{2+}$/1,1′-dimethyl-4,4′-bipyridinium (MV^{2+}) system[35] as measured by pulse laser spectrochemical means. Parameter ϕ_{CE} is given by $\phi_{CE} = k'_1/(k'_1 + k_{-1})$ (see eqs 2b and 2c); this allows calculation of values of $k'_1/k_{-1} = 0.14$ (Figure 8 data) and 0.08 (Figure 10 data), average = 0.11, indicating that the physical quenching process is ∼9× faster than the chemical quenching process. It can be seen from eqs 2 that successful production of $Ru(bipy)_3^{3+}$ and Fe^{2+} has three key steps: (i) formation of $Ru(bipy)_3^{2+}*$ from $Ru(bipy)_3^{2+}$, efficiency described by ϕ; (ii) formation of $[Ru(bipy)_3^{2+}\cdots Fe^{3+}]*$ from $Ru(bipy)_3^{2+}$, efficiency described by k_1/k_0; (iii) formation of $Ru(bipy)_3^{3+}$ and Fe^{2+} from $[Ru(bipy)_3^{2+}\cdots Fe^{3+}]*$, efficiency described by k'_1/k_{-1};

From Table 2, it can be seen that it is the last of these that is least efficient and so is the key step in determining the overall efficiency of primary redox product generation in the $Ru(bipy)_3^{2+}/Fe^{3+}$ system.

It can be shown from eqs 19 and 20 that the maximum concentration of S* generated in these experiments is given by $[S^*]_{max} = \phi I_{ph}\epsilon_\lambda[S]/k_0$. For the data of Figure 7, this gives $[Ru(bipy)_3^{2+}*]_{max} = 4.7 \times 10^{-7}\ mol\ m^{-3}$, which is substantially less than the smallest concentration of the scavenger Fe^{3+} used in that experiment (1 mol m^{-3}), confirming the validities of assumptions 1.1 and 2.2. Noting that $X_{k,2} = (D_{Ru}/k_2)^{1/2}$, then from the data of Table 2, a value of $X_{k,2} = 49$ μm may be obtained. The maximum concentration of sensitizer used in the experiments of Figures 7−10 was 2 mol m^{-3} which, in accordance with eq 6b, gives a minimum value of $X_\epsilon = 73$ μm. Thus, for all experiments reported herein, $X_{k,2} < X_\epsilon$, confirming the validity of the assumption underpinning the derivations of eqs 7a and 22a.

4. Conclusions

We have demonstrated that it is possible to prepare and characterize very thin ring MOREs with a/b values >0.99. We have also established that it is possible to use such MOREs to study the wavelength dependence of photocurrents derived from photoelectrochemically active systems, demonstrating the potential utility of the MORE as a selective spectrophotoelectrochemical analytical probe.

We have demonstrated that it is possible to derive asymptotic analytical expressions for the time dependence of the diffusion limited transient light-on photocurrent generated by PE and PCE systems at very thin ring MOREs. The expressions were generated by solving, in Laplace space, the time-dependent diffusion equation for the photogenerated electroactive species both inside and outside the beam and matching solutions at the beam surface. The expressions are used to design experimental protocols that allow for the characterization of the system's kinetics. The MORE, the expressions, and the associated protocols will therefore be useful not only as an analytical tool but also in kinetic studies of a range of homogeneous and microheterogeneous (e.g., colloidal semiconductors) photoelectrochemical systems.

The expressions were tested by using them to interpret the results of a MORE study of the kinetics of the $Ru(bipy)_3^{2+}/Fe^{3+}$ PCE system. The values of the Stern−Volmer coefficient for the system, $K_{SV} = 2.05\ m^3\ mol^{-1}$, and the efficiency for the primary redox products $Ru(bipy)_3^{3+}$ and Fe^{2+} escaping cage recombination, $\phi_{CE} = 0.099$, compare favorably with values for analogous processes in the literature. We are currently using the MORE to study the photogeneration and electrochemistry of the short-lived singlet oxygen species produced by the photoexcitation of sensitizing dyes such as rose Bengal and methylene blue.

Acknowledgment. We thank the University of Central Lancashire (UCLan) for a postgraduate research assistantship for F.A. and a period of Sabbatical leave for C.B. We also thank the EM Facility at the University of Brighton for help with the manufacture of the MOREs.

Supporting Information Available: The following information is available: S1, detailed experimental methods, including MORE fabrication; S2, electrochemical characterization of very thin ring MOREs in the dark; S3, a description of the simplification of eq 12; S4, the derivation of eq 14; S5, a discussion of the identity of the reducing agent associated with reaction 2d. This material is available free of charge via the Internet at http://pubs.acs.org.

References and Notes

(1) Pennarun, G. I.; Boxall, C.; O'Hare, D. *Analyst* **1996**, *121*, 1779.
(2) Andrieux, F. P. L.; Boxall, C.; O'Hare, D. *J. Electroanal. Chem.* **2006**, *589*, 177.
(3) Berenguier, B.; Lewerenz, H. J. *Electrochem. Comm.* **2006**, *8*, 165.
(4) Gratzel, M. *Inorg. Chem.* **2005**, *44*, 6841.
(5) Figgemeier, E.; Hagfeldt, A. *Int. J. Photoenergy* **2004**, *6*, 127.
(6) Lewis, N. S. *J. Electroanal. Chem.* **2001**, *508*, 1.
(7) Qamar, M.; Muneer, M.; Bahnemann, D. *Res. Chem. Intermed.* **2005**, *31*, 807.
(8) LeGurun, G.; Boxall, C.; Taylor, R. T. The Application of Photocatalysis in Transition Metal and Actinide Redox Chemistry. *Recent Research Developments in Photochemistry and Photobiology*; Transworld Research Network: Trivandum, India, 2004; Vol. 7, p 39.
(9) Mills, A.; Hill, G.; Crow, M.; Hodgen, S. *J. Appl. Electrochem.* **2005**, *35*, 641.
(10) Kishida, H.; Hirota, K.; Wakabayashi, T.; Okamoto, H.; Lee, B. L.; Kokubo, H.; Yamamoto, T. *Synth. Met.* **2005**, *153*, 141.
(11) Staskowiak, E.; Dudkowiak, A.; Hanyz, I.; Wiktorowicz, K.; Frackowiak, D. *J. Photochem. Photobiol., A* **2004**, *163*, 127.
(12) Legeai, S.; Chatelut, M.; Vittori, O. *Electrochim. Acta* **2005**, *50*, 4089.
(13) Lakard, B.; Jeannot, J. C.; Spajer, M.; Herlem, G.; de Labachelerie, M.; Blind, P.; Fahys, B. *Electrochim. Acta* **2005**, *50*, 1863.
(14) Melville, J. L.; Simjee, N.; Unwin, P. R.; Coles, B. A.; Compton, R. G. *J. Phys. Chem. B* **2002**, *106*, 10424.
(15) Lee, Y.; Amemiya, S.; Bard, A. J. *Anal. Chem.* **2001**, *73*, 2261.
(16) Szabo, A. *J. Phys. Chem.* **1987**, *91*, 3108.
(17) Symanski, J. S.; Bruckenstein, S. *J. Electrochem. Soc.* **1998**, *135*, 1985.
(18) Fleishmann, M.; Pons, S. *J. Electroanal. Chem.* **1987**, *222*, 107.
(19) Fleishmann, M.; Bandyopadhyay, S.; Pons, S. *J. Phys. Chem.* **1985**, *89*, 5537.
(20) Philips, C. G.; Stone, H. A. *J. Electroanal. Chem.* **1995**, *396*, 277.
(21) Cope, D. K.; Tallman, D. E. *J. Electroanal. Chem.* **1991**, *303*, 1.
(22) Cope, D. K.; Scott, C. H.; Tallman, D. E. *J. Electroanal. Chem.* **1989**, *289*, 49.
(23) Kalpathy, U.; Tallman, D. E. *J. Electroanal. Chem.* **1992**, *325*, 65.
(24) Tallman, D. E. *Anal. Chem.* **1994**, *66*, 557.
(25) Wu, Z.; Zhang, Z. *Acta Chim. Sin.* **1993**, *51*, 239.
(26) Wu, Z.; Zhang, Z. *Acta Chim. Sin.* **1993**, *51*, 697.
(27) Brookes, B. A.; Gavaghan, D. J.; Compton, R. G. *J. Phys. Chem. B* **2002**, *106*, 4886.
(28) Pennarun, G. I.; Boxall, C.; O'Hare, D. Extended Abstract. *Proceedings of the Symposium on Chemical and Biological Sensors and Analytical Electrochemical Methods*; 192nd Meeting of the Electrochemical Society, Sept 1997; The Electrochemical Society: Pennington, NJ, 1997; p 1039.
(29) Andrieux, F. P. L.; Boxall, C.; Xiao, S.; O'Hare, D. Extended Abstract. *Proceedings of the Symposium on Chemical and Biological Sensors and Analytical Methods II*; 200th Meeting of the Electrochemical Society, Sept 2001; The Electrochemical Society: Pennington, NJ, 2001; pp 531.
(30) Albery, W. J.; Foulds, A. *J. Photochem.* **1979**, *10*, 41.
(31) Paris, J. P.; Brandt, W. W. *J. Am. Chem. Soc.* **1959**, *81*, 5001.
(32) Lin, C. T.; Sutin, N. *J. Phys. Chem.* **1976**, *80*, 97.
(33) Abramowitz, M.; Stegun, I. A. *Handbook of Mathematical Functions*; Dover Publications: New York, 1965; p 1020.
(34) Navon, G.; Sutin, N. *Inorg. Chem.* **1974**, *13*, 2159.
(35) Orellana, G.; Braun, A. M. *J. Photochem. Photobiol., A* **1989**, *48*, 277.
(36) In house rotating disk electrode measurements.